scientific reports

Check for updates

OPEN

Synergistic growth suppression of *Fusarium oxysporum* MLY127 through Dimethachlon Nanoencapsulation and co-application with *Bacillus velezensis* MLY71

Lei Yang[1], Juntao Gao[2], Dong Xiang[1], Xinyu Hu[1], Guan Lin[2] & Yong Liu[2]✉

Fusarium **oxysporum is a destructive plant pathogen with robust survival mechanisms, complicating control efforts. This study aimed to develop nanoformulated fungicides, screen antagonistic bacteria, and evaluate their combined efficacy. A novel self-emulsifying nanoemulsion (DZW) was formulated using zein and benzaldehyde-modified wheat gluten (BgWG) as carriers for dimethachlon (DTN). The preparation process optimized material ratios and emulsification techniques. Concurrently, antagonistic bacterial strains against *F. oxysporum* were screened via the plate standoff method, identifying *Bacillus velezensis* MLY71 as both antagonistic and compatible with DTN. The DZW nanoemulsion achieved a particle size of 93.22 nm, an encapsulation efficiency (EE) of 90.57%, and a DTN loading capacity (LC) of 67.09%, with sustained release over 96 h. The combination of DTN (0.04 mg·mL^{-1}) and *B. velezensis* MLY71 (1 × 10^{4} CFU·mL^{-1}) achieved a 76.66% inhibition rate against *F. oxysporum* MLY127, 1.71 times greater than DTN alone, indicating significant synergy. At a DTN concentration of 0.20 mg·mL^{-1}, the combination of DZW and MLY71 showed a synergy coefficient of 1.33. This synergy was also observed in soil environments, indicating its adaptability for controlling soil-borne pathogens. As sustainable management continues to gain attention in agricultural disease control, this study offers a promising strategy for achieving higher efficacy with the same fungicide dose or satisfactory control with reduced fungicide application. The excellent drug-loading performance of BgWG also expanded the applications of the wheat by-product gluten.**

Keywords *Bacillus velezensis*, Dimethachlon, *Fusarium oxysporum*, Growth suppression, Nanoencapsulation, Synergistic strategy

Fusarium represents a group of globally widespread fungal pathogens that can cause severe diseases in a variety of crops, posing a significant threat to the production of cereal crops and vegetables. Common pathogens within the *Fusarium* genus include *F. graminearum*, *F. oxysporum*, and *F. solani*. *F. oxysporum*, in particular, is known to rely primarily on seeds and soil for transmission and can persist for extended periods in the form of chlamydospores when a host is absent[1,2]. This pathogen has a host range that encompasses over 100 types of plants, including vegetables, flowers, and cotton. It inflicts wilting on plants by colonizing vascular bundles, thereby posing a serious risk to agricultural production[3]. Currently, chemical fungicides remain the preferred choice for plant disease control and pest control in agriculture[4,5]. However, with the growing emphasis on green agriculture and environmental awareness, there is an increasing focus on enhancing the efficacy of fungicides to reduce the amount of chemical fungicide applied. The development of more effective disease management strategies, such as the synergistic strategy of combining pesticides and beneficial microbes discussed in this study, is an urgent necessity that aligns with the principles of green and sustainable agricultural development[6].

[1]China Tobacco Hunan Industrial Co. Ltd, Changsha, China. [2]School of Biological & Chemical Engineering, Zhejiang University of Science & Technology, Hangzhou, China. ✉email: 116047@zust.edu.cn

The swift advancement of nanotechnology has been, and will remain, instrumental across various sectors such as materials science, biomedicine, agriculture, and industry[7]. In agriculture, nanotechnology has shown promising results, including the efficient delivery of insecticidal substances, enhancement of plant health, extension of the effectiveness period, reduction in the application of fungicides, and mitigation of environmental fungicides pollution. The synergistic delivery effects that nanoparticles offer to chemical or biological fungicide are particularly encouraging for the development of more fungicide nanoformulations[8,9]. Dimethachlon (DTN, CAS No. 24096-53-5) is a broad-spectrum, low-toxicity, systemic fungicide that has proven effective against a variety of fungal diseases, such as rice sheath blight caused by *Rhizoctonia solani Kuhn*, rape sclerotinia rot caused by *Sclerotinia sclerotiorum*, and tobacco brown spot disease caused by *Alternaria alstroemeriae*. It also has good effects on a variety of *F. oxysporum* diseases. By nanoembedding and controlling the release of DTN, its inhibitory effect can be enhanced, which may help in reduce the amount of fungicide applied, thereby improving food safety and environmental sustainability. Furthermore, the combination of biocontrol strains with chemical fungicides can also offer unique ecological benefits: chemical fungicides can assist biocontrol strains in overcoming the soil ecological environment, allowing them to establish and gain a population advantage. In this process, chemical fungicides provide a rapid, short-term control effect, establishing an early advantage for biocontrol strains. As biocontrol strains subsequently colonize the plant root system, they may continuously secrete biocontrol active ingredients and growth factors, and induce some anti-disease responses in the plant. This complementary approach involving chemical fungicides and biocontrol strains offers a new perspective for the sustained and efficient management of diseases[10,11].

In this study, we first explored the development of DTN nanoformulations to enhance their antifungal effects. Second, antagonistic microbial species compatible with DTN were screened. Finally, through the combined application of DTN nanoformulations and the antagonistic microbe, synergistic growth inhibition against *F. oxysporum* MLY127 was achieved. The specifics of our research are outlined as follows.

Materials and methods

Materials and instruments

Zein, ethanol (95%, V/V), n-butanol, ethyl acetate, hexylamine, and benzaldehyde (BZH) were AR-grade and were obtained from Shanghai Sinopharm Group Chemical Reagent Company Limited (Shanghai, China); Dimethachlon (DTN) was of industrial grade and was purchased from Huizhou Minko Biotechnology Co. (Quzhou, Zhejiang, China). High-performance liquid chromatography (HPLC, Waters e2695 with a Waters 2489 UV detector and column SunfireTM C18 (250 × 4.6 mm, 5 μm)) was obtained from Waters Corporation (MA, USA). The scanning electron microscope (SEM) SU1510, transmission electron microscope (TEM) HT7700 Exalens and fluorescence spectrophotometer F-1000 for the analysis were obtained from Hitachi (Mitoshi, Japan). A thermogravimetric analyzer (TGA) STA 449 F3 was obtained from Netzsch (Selb, Germany). A UV-5500 ultraviolet spectrophotometer from Shanghai Yuan'an Analytical Instruments Co (Shanghai, China) was used. A Zetasizer-Nano-ZS nanoparticle size potential analyzer from Malvern Instruments (Worcestershire, UK) was used. An X-ray diffractometer DX-2700 from Hoyuan Instruments Ltd (Dandong, Liaoning, China) was used. The FTIR spectrometer (FTIR) Vertex-70 was from Bruker (Karlsruhe, Germany). *F. oxysporum* MLY127 was isolated from the stem of diseased tobacco plants collected from farm field (105°60′E, 27°15′N) located in Guizhou, China in August 2023; MLY64, MLY71, and MLY85 were isolated from a soil sample collected from farm field (104°51'E, 24°38'N) located in Guizhou, China, at May 2022 and were stored at the Agricultural Microbial Engineering Laboratory of Zhejiang University of Science and Technology.

Modification of wheat gluten with benzaldehyde

The BZH solutions were prepared by adding BZH to H_2O (100 mL) in quantities of 0.075, 0.125, 0.175, 0.225, and 0.275 moles, respectively. Then, 20 g of WG was accurately weighed and added to each BZH solution. The mixtures were stirred on a magnetic stirrer at room temperature for 4 h, resulting in products (BZH grafting-modified wheat gluten, BgWG) labeled BgWG1 to BgWG5 according to the BZH quantities of 0.075 to 0.275 moles. After stirring, each mixture was centrifuged at 3,000 rpm·min^{-1} for 15 min at 25 °C, the supernatant was discarded, and the pellets were freeze-dried overnight and ground into powder for use.

Measurement of the solubility of BgWG

To determine the water solubility of BgWG, a 1% sample mixture was prepared, equilibrated for 30 min, and then centrifuged at 3,000 rpm·min^{-1} for 30 min at 25 °C. One milliliter of the supernatant and 4 mL of biuret reagent were mixed together and shaken vigorously for 10 min. The absorbance at 540 nm was subsequently measured via a UV spectrometer after 30 min of standing[12]. The solubility was calculated via the standard curve established via the method of Garrido[13] (details are shown in Figure S1 of the Supplementary Material). For alcohol solubility, a 1% sample solution in 95% ethanol was prepared and the same procedure as for water solubility was performed.

Measurement of the emulsifying properties of the BgWG

A BgWG sample suspension was prepared at 10 mg·mL^{-1} in a total volume of 40 mL. Then, 10 mL of soybean oil was added in and mixed thoroughly for 1 min via a high-speed disperser at 25 °C and 10,000 rpm·min^{-1}. Samples were taken from the bottom of the emulsion at 0 min and 10th min after emulsification. The samples were then diluted 100 times in 0.1% SDS, and the absorbance was measured at 500 nm with an ultraviolet spectrophotometer (A_{500}). A 0.1% SDS served as the blank control[14]. The emulsifying activity index (EAI) and emulsion stability index (ESI) of wheat gluten were determined via the following formulas.

$$\mathrm{EAI}\left(\mathrm{m}^2/\mathrm{g}\right) = \frac{\mathrm{n} \times 2 \times 2.303 \times \mathrm{A}_{500} \times 10^{-4}}{\phi\ \mathrm{CL}} \quad (1)$$

n: number of dilutions; ϕ : the oil phase as a fraction of the system is 0.2; C: protein concentration ($g{\cdot}mL^{-1}$); L: optical diameter of colorimetric cell (cm).

$$\mathrm{ESI} = \frac{\Delta\,\mathrm{T} \times \mathrm{A}_0}{\mathrm{A}_0 - \mathrm{A}_\mathrm{t}} \quad (2)$$

A_0: absorbance value at 0 min; A_t: absorbance value at t min.

FTIR determination of BgWG

The sample powder and potassium bromide at a mass ratio of 1:15 were weighed and ground into powder, and then 50.0 mg of powder was weighed accurately and placed under pressure. The powder was pressed into a translucent homogeneous sheet, and the sample was placed under an infrared spectrometer and scanned for determination. The atmospheric background was used as the background, the scanning frequency was 500 ~ 4,000 cm^{-1}, the number of scans was 32, and the resolution was 4 cm^{-1}.

Preparation and optimization of a DTN-loaded nanoemulsion formulation

The 2.0 g of DTN was precisely weighed and mixed with specific amounts of Zein and BgWG3 (Table 1). This mixture was then combined with 100 mL of a 90% ethanol solution and stirred at 900 $rpm{\cdot}min^{-1}$ for 30 min to ensure the complete dissolution of DTN, Zein and BgWG3 in ethanol. A cosurfactant (n-Butanol) was added to the mixture, which was stirred at 900 $rpm{\cdot}min^{-1}$ for an additional 10 min. Subsequently, 400 mL of dH_2O was added, and the mixture was stirred at 1,200 $rpm{\cdot}min^{-1}$ for 40 min to form the DZW nanoemulsion preparation. The DZW nanoemulsion was then centrifuged at 8,000 $rpm{\cdot}min^{-1}$ for 30 min at 25 °C. The supernatant was reserved for subsequent assays of EE and LC, while the pellet, consisting of DZW nanomicrocapsules, was freeze-dried for further characterization. The preexperimental screening process is described in Tables S1, S2, and S3 of the Supplementary Material.

Determination of the particle size and zeta potential of DZW nanomicrocapsules

A 0.1 mL of sample was diluted 200 times, and 10 μL of the diluted solution was added to dH_2O to disperse the sample emulsion to determine the particle size, polydispersity coefficient (PDI) and zeta-potential of the samples via a nanoparticle size potential analyzer[15]. Three parallel tests were performed in each group and the data obtained are expressed as the means ± standard deviations.

Determination of the EE and LC of DZW nanomicrocapsules

The DTN content was determined via HPLC (see Figure S5 in the Supplementary Material for the assay method and standard curve), and on the basis of the standard curve, the mass of the net DTN in the supernatant was calculated on the basis of the peak area and was recorded as the mass of the free DTN. The precipitate obtained by centrifugation was freeze-dried and weighed, recorded as the mass of nanomicroencapsulated particles, and used for other analyses. The EE and LC of DTN were calculated as follows:

$$\mathrm{EE}\ (\%) = \frac{\text{Total mass of DTN} - \text{Mass of free DTN}}{\text{Total mass of DTN}} \times 100 \quad (3)$$

$$\mathrm{LC}\ (\%) = \frac{\text{Total mass of DTN} - \text{Mass of free DTN}}{\text{Mass of DZW nano} - \text{microencapsulated particles}} \times 100 \quad (4)$$

XRD analysis

X-ray diffraction (XRD) was used to analyze the crystal structure of the lyophilized nanocrocapsule samples. A certain mass of freeze-dried sample was taken into the sample tank and flattened. The range of the scanning diffraction angle was 0 ~ 60°, and the sample was continuously scanned with a step size of 0.04°.

Sample name	DTN (g)	Zein (g)	BgWG3 (g)	*n*-Butanol (g)	Ethanol (mL)	dH_2O (mL)
DZW1	2	0	0	0	100	400
DZW2	2	1	0	0	100	400
DZW3	2	1	0	1	100	400
DZW4	2	0.9	0.1	1	100	400
DZW5	2	0.7	0.3	1	100	400
DZW6	2	0.5	0.5	1	100	400
DZW7	2	0.3	0.7	1	100	400

Table 1. Optimization and screening of the DZW formulation for the DTN.

Microscopic morphology analysis of DZW nano-microencapsulated particles

TEM was used to observe the microstructure of DZW the nano-microcapsules. The 100 μL of each DZW nanoemulsion was diluted 100 times, and a solution droplet was transferred onto a copper grid with a capillary tube, air-dried for 3 min, stained with a concentration of 1.5% uranyl acetate, left to air dry, and then subjected to TEM to observe the micromorphological features[16]. The surface morphologies of the nanoparticles were observed suing SEM. The nanoemulsion samples were diluted for about 100 times, dropped on a single-sided polished silicon wafer and left to dry at room air. After gold sputtering treatment, the samples were subjected to SEM for observation at a magnification of 60,000 times.

Fluorescence spectrometry analysis

The fluorescence spectra of the DZW samples were analyzed at 25 °C using a Hitachi F-1000 fluorescence spectrophotometer. Before measurement, the test samples were diluted to a protein concentration of 0.2 mg·mL^{-1} to obtain a suitable signal intensity. The excitation wavelength was 280 nm, the scanning speed was 1,200 nm·min^{-1}, the acquisition wavelength range was 290–500 nm, and the excitation and emission wavelength slit width was 5 nm.

TGA analysis

The TGA tests of the samples were carried out on a thermogravimetric analyzer. The samples were accurately weighed from 5 to 10 mg, and nitrogen was used as the equilibrium gas and sample gas, with a heating rate of 20 °C·min^{-1}, a starting temperature of 50 °C, and a termination temperature of 500 °C.

Test of DTN release characterization

The release behavior of DTN was assessed via dynamic dialysis[17]. The nanoemulsion was thoroughly mixed, and 50 mL was placed into a pretreated dialysis bag with a molecular weight cutoff of 8,000 Daltons. The bag was immersed in 200 mL of a methanol/water (70:30, V/V) release medium in a 500 mL conical flask, and then placed in a ZQLY-180 N incubator shaker with 100 rpm·min^{-1} shaking at 28 ± 2 °C. At regular intervals, 1 mL of the release medium was sampled from outside the bag, and an equal volume of the methanol/water mixture was added to maintain a consistent release medium volume. The DTN content was detected via HPLC. Three parallel trials were performed for each test and the values obtained are expressed as the means ± standard deviations. Release curves were plotted and analyzed for their characteristics.

$$\text{Release rate } (\%) = \frac{\text{Net mass of Dimethachlon in the release medium solution}}{\text{Net total mass of Dimethachlon}} \times 100 \quad (5)$$

Screening of biocontrol strains against *F. oxysporum* MLY127

The agar plate antagonism assay was applied for biocontrol strain screening: *F. oxysporum* MLY127 colonies were grown on PDYH solid media (potato flour, 6.0 g; dextrose, 20.0 g; agar, 20.0 g; yeast extract, 6.0 g; dH$_2$O, 750 mL; pH = 5.6 ± 0.2; humic acid, 50.0 g; dH$_2$O, 250 mL; and two separate autoclave sterilization, mixing and cooling to obtain the PDYH solid media.) for 4 ~ 5 days before use. Approximately 5 × 5 mm mycelial agar plugs were excised from the colony edges and inoculated to the PDYH plate periphery, approximately 1.5 cm from the Petri dish edge. The bacterial biocontrol strains were then inoculated along the plate diameter approximately 5 cm from the MLY127 colony (Petri dish diameter 9 cm). The inoculated plates were incubated at 30 °C for 5 to 7 days. The plates inoculated with only MLY127 were prepared as a negative control. The presence and size of the inhibition zone were observed to screen for bacterial strains exhibiting an antagonistic effect. Three parallel trials were conducted for each set of tests.

Growth inhibition of *F. oxysporum* MLY127 by a combination of DZW and *B. velezensis* MLY71

The inhibitory effect of *B. velezensis* MLY71 combined with DZW against *F. oxysporum* MLY127 was evaluated via a mycelial growth rate assay[18]. *B. velezensis* MLY71 was cultured in LB liquid medium at 30 °C for 48 h. The *B. velezensis* MLY71 cells were then suspended in sterilized water and added to PDYH solid media once the media had cooled to approximately 40 °C (after autoclaving at 121 °C for 30 min). The concentration of *B. velezensis* MLY71 cells ranged from 1×10^8 to 1×10^4 CFU·mL^{-1}. The DZW nanoemulsion was added in PDYH medium at the DTN concentrations of 0.40, 0.20, and 0.04 mg·mL^{-1}, creating composite solid media. The fresh *F. oxysporum* plugs (5 × 5 mm) were inoculated at the center of each plate. Controls included treatments with the DZW nanoemulsion or *B. velezensis* suspension alone, and a blank control without either. Each treatment was replicated three times, and the samples were incubated at 30 °C for 7 days. Colony diameters were measured via the cross-plate method, and the inhibition rate (%) was calculated.

$$\text{Mycelial growth inhibition rate } (\%) = \frac{(\mathrm{C} - \mathrm{d}) - (\mathrm{T} - \mathrm{d})}{C - d} \times 100 \quad (6)$$

d: Diameter of fungal cake; C: Diameter of fungal growth on untreated PDYH; T: Diameter of fungal growth on treated PDYH.

Evaluation of the synergistic effects of the combination of DZW5 and *B. velezensis* MLY71

The inhibitory effect of the combination of DZW5 and *B. velezensis* MLY71 against *F. oxysporum* MLY127 was tested via the plate standoff method on PDYH medium. The DZW nanoemulsion was diluted to three different concentrations in sterilized water and mixed with PDYH solid medium. The plate standoff method was adopted.

A control group in which PDYH medium without the addition of the DZW nanoemulsion or *B. velezensis* MLY71 was used to monitor the growth of *F. oxysporum* MLY127 and the extent of the antagonistic zone.

The synergistic coefficient was occupied to evaluate the preventive effect of the system of fungicide-biocontrol bacteria, and the formula was calculated as follows[19]:

$$\text{Synergy factor (S)} = \frac{R_{Bt} - R_{BCK}}{R_{Tt} - R_{TCK}} \quad (7)$$

R_{BCK}: radius of control colony of *F. oxysporum*; R_{TCK}: radius of control colony of *B. velezensis*; R_{Bt}: radius of confrontation colony of *F. oxysporum*; R_{Tt}: radius of confrontation colony of *B. velezensis*. If $S \geq 1.5$, the synergy between the biocontrol strain and fungicide has a synergistic effect; if $1.5 > S \geq 1$, the synergy between the biocontrol strain and fungicide has an additive effect; if $S < 1$, the synergy between the biocontrol strain and fungicide has an antagonistic effect.

Efficacy test of DZW5 plus *B. velezensis* MLY71 against *F. oxysporum* MLY127 in soil

An indoor efficacy test of DZW5 plus *B. velezensis* MLY71 against *F. oxysporum* MLY127 in soil was conducted under strictly controlled conditions. A total of 360 g of sterilized air-dried soil was divided into 36 portions (10 g per portion) and placed in Petri dishes with a diameter of 9 cm. The combinations of DZW emulsion and *B. velezensis* MLY71 culture were applied in the form of an aqueous solution, with the following doses: DTN at 0, 0.04, and 0.4 mg kg^{-1} d.m.soil, and *B. velezensis* MLY71 at 0, 10^4, 10^6, and 10^8 CFU kg^{-1} d.m.soil. Simultaneously, the soil water content was adjusted to 50% using sterilized distilled water and then an approximately 5 × 5 mm *F. oxysporum* block was inoculated at the center of each Petri dish. The Petri dishes were cultured in a constant-temperature incubator at 30 °C for 7 days to observe the mycelial growth differences of *F. oxysporum*. Three parallel trials were conducted for each set of variables.

Data analysis

Graphs were plotted via Origin 8.5 software (OriginLab Co., Northampton, MA, USA), and analysis of variance (ANOVA) and analysis of significance of differences (ANOVA) were performed via IBM SPSS Statistics 26.0 software (SPSS Inc., Chicago, IL, USA). Each set of experiments was replicated three times in parallel, and the results obtained are expressed as the means ± standard deviations. The strain identification methods and phylogenetic tree plots are shown in Supplementary Material Figure S8.

Results

FTIR analysis indicated N-H grafting and secondary structure transformation of BgWG

The N-H stretching vibration in wheat gluten molecules produces a strong, broad absorption peak between 3300 and 3400 cm^{-1} (Fig. 1). The characteristic peaks at 1700 − 1600, 1580 − 1480, and 1350 –1200 cm^{-1} are attributed to the amide I (C = O stretching vibration), amide II (N-H deformation vibration, C-N stretching vibration), and amide III bands, respectively[20]. The strength of the 3300–3500 cm^{-1} peak decreased step by step with increasing amounts of BZH from samples BgWG1 to BgWG5, indicating a reduction in the number of primary amine groups after BZH grafting. Moreover, the increased absorption peaks at 3075 cm^{-1} and 1455 cm^{-1}, corresponding to C = C stretching and deformation vibrations on the benzene ring, and the new peak at 744 cm^{-1} due to the out-of-plane deformation vibration of the monosubstituted benzene ring skeleton, confirmed the successful grafting of the benzyl group onto the amino group. However, the newly formed C = N bond shares a similar stretching vibration peak with the C = O bond at approximately 1650 cm^{-1}; therefore, no obvious peak change was observed.

Figure 2 shows the proportions of each secondary structure in wheat gluten before and after modification. Due to the introduction of characteristic peaks in the amide I band from the BZH treatment of wheat gluten in this study, structural analysis may be affected. However, the peaks in the amide III band (1330 –1220 cm^{-1}) have been clearly recognized in recent years. This study utilizes Peak Fit v4.12 (California, USA) and Omnic software (Massachusetts, USA) to analyze the amide III band spectra. The absorption peaks correspond to specific secondary structures, such as α-helices (1330 –1290 cm^{-1}), β-sheets (1250 –1220 cm^{-1}), β-turns (1295 –1265 cm^{-1}), and random coils (1270 –1245 cm^{-1}), with other wavelengths indicating interactions between adjacent structures[21]. Upon benzaldehyde modification, the β-sheet content of BgWG3 decreased to 35.76% from 53.44% content in raw wheat gluten. After modification, the α-helix content remained relatively stable (24.93% vs. 26.98%), suggesting that benzaldehyde-grafting did not destabilize but slightly enhanced the wheat protein structure. Since the α-helices are known for their compact, cavity-free structure and greater stability, an increase in their content indicates greater overall protein stability[22]. Both β-turns and random coils significantly increased, from 13.22% and 8.41–23.67% and 13.59%, respectively. Those β-turns and random coils are more flexible, allowing for group stretching and alterations in the molecular structure, which lead to better exposure of hydrophilic groups in proteins and, consequently, an increase in their solubility.[23].

The BgWG exhibited improved solubility, emulsification and emulsion stability

The experimental results were derived from the soluble protein content in solution on the basis of the linear correlation between the soluble protein concentration and absorbance (as shown in Figure S1). The solubility of BgWG was significantly enhanced in both water and alcohol (Fig. 3), likely due to alterations in the stretching of hydrophobic groups and protein sheeting after modification[24], as well as increased interactions between hydrophilic side chain groups and water, which improved both the water solubility of BgWG[25] and its emulsification performance (Fig. 3). Optimal water solubility, emulsification ability, and emulsion stability were achieved with BgWG3, which was selected as the optimized material for subsequent use.

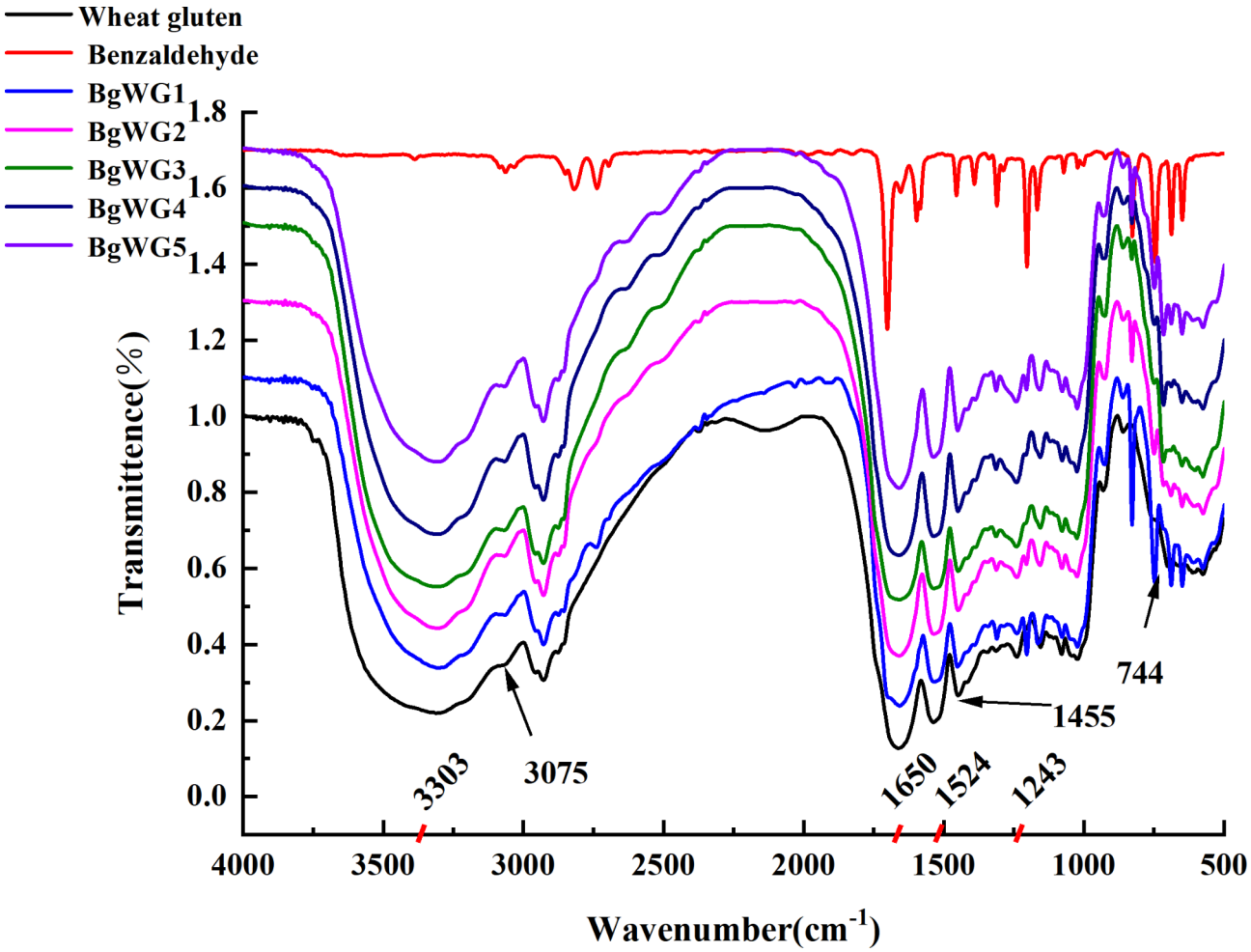

Fig. 1. Infrared spectra of gluten modified with different concentrations of BZH.

The optimal combination of zein,n-butanol, and BgWG resultedin particle sizes below 100 nm and strong zeta potentials.

Through preliminary screening of encapsulation materials and cosurfactants, Zein and n-butanol were found to be more suitable for the preparation of DTN-loaded nanoemulsions (results shown in Figures S2, S3, and S4 of the Supplementary Material). Further optimization experiments of the amounts of zein, n-butanol, and BgWG showed that at a DTN-to-zein mass ratio of 2:1, the particle size decreased to 192.60 nm with a PDI < 0.3 (Fig. 4), indicating a uniform particle size distribution within the emulsion. In contrast, the particle size of DTN in ethanol without zein addition (sample DZW1) reached 954.78 nm with a PDI > 0.3, indicating a heterogeneous solution. The subsequent addition of n-butanol (sample DZW3) further reduced the particle size by reducing interfacial tension, decreasing interface rigidity, enhancing interfacial film mobility, and adjusting the HLB value of the surfactant during emulsification[26]. By adjusting the ratio of zein to BgWG, the nanoparticle size was further minimized, reaching 93.22 nm at a zein-to-BgWG3 mass ratio of 7:3. This reduction may be attributed to the unfolding of BgWG molecular chains, exposing more hydrophobic groups, thereby altering surface hydrophobicity and influencing interfacial adsorption and interactions, which in turn reduces the particle size. Meanwhile, overaddition of BgWG (Sample DZW7) might disrupt emulsion interactions, increasing the nanoparticle size and causing heterogeneity in the emulsion. Zeta potentials were shown in Fig. 4. DTN has a negative charge, whereas Zein is positively charged because the pH of the solution is below its isoelectric point (pH = 6.8)[27]. The zeta potentials of DTN-loaded nanoparticles ranged from + 16.57–20.30 mV, resulting in strong repulsion between particles, and leading to better dispersion and a more stable system[28,29]. The addition of BgWG3 did not significantly affect the zeta potential of the nanoemulsion.

DTN was efficiently encapsulated and loaded into composite nanoparticles

The EE and LC of the DTN-loaded nanoemulsion were calculated from the measured chromatographic peak areas (the linear relationship between the DTN concentration and peak area is detailed in Supplementary Material Figure S5). Figure 5 displays the EE and LC for DZW1-DZW7, with prescreening data presented in Supplementary Material Figure S6. The nanoparticles were well encapsulated, generally showing high EE and LC, with DZW5 performing the best at 90.57% EE and 67.09% LC. The lower EE for DZW7 could be due to

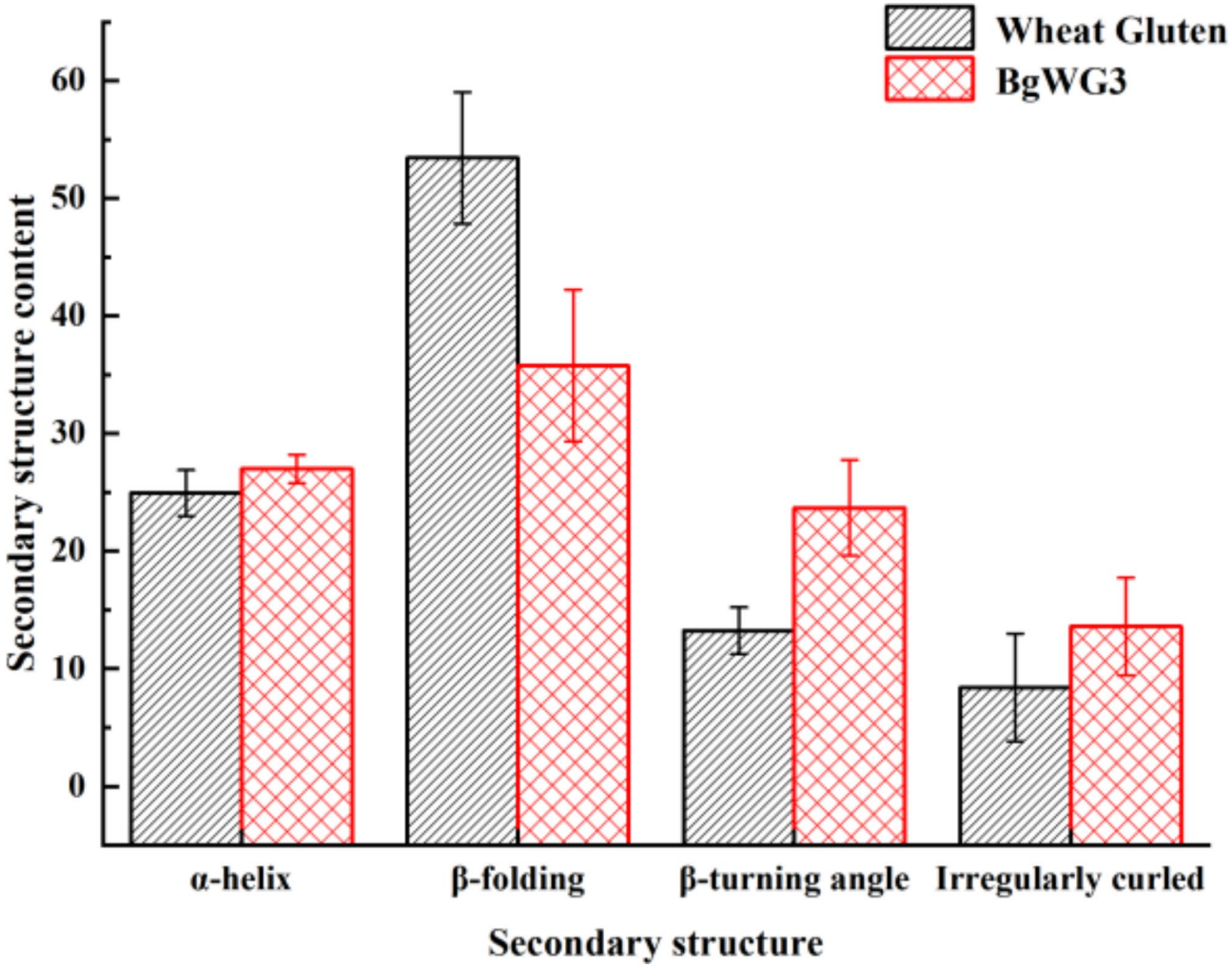

Fig. 2. Comparison of protein secondary structure before and after modification.

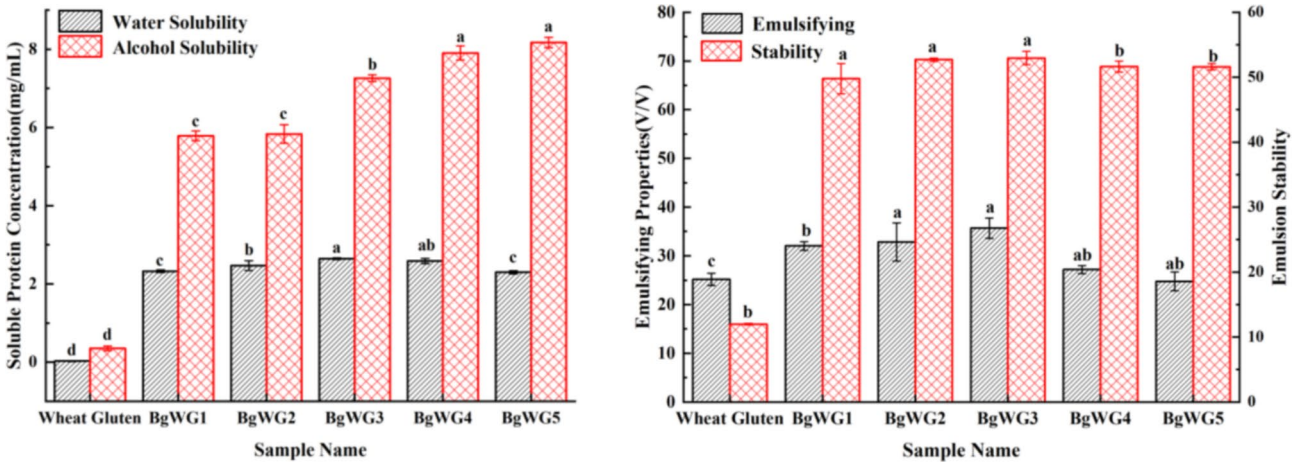

Fig. 3. Solubility, emulsifying and emulsion stabilizing ability of BgWG samples. The lowercase letters in the graph represent significant differences between formulations ($p < 0.05$).

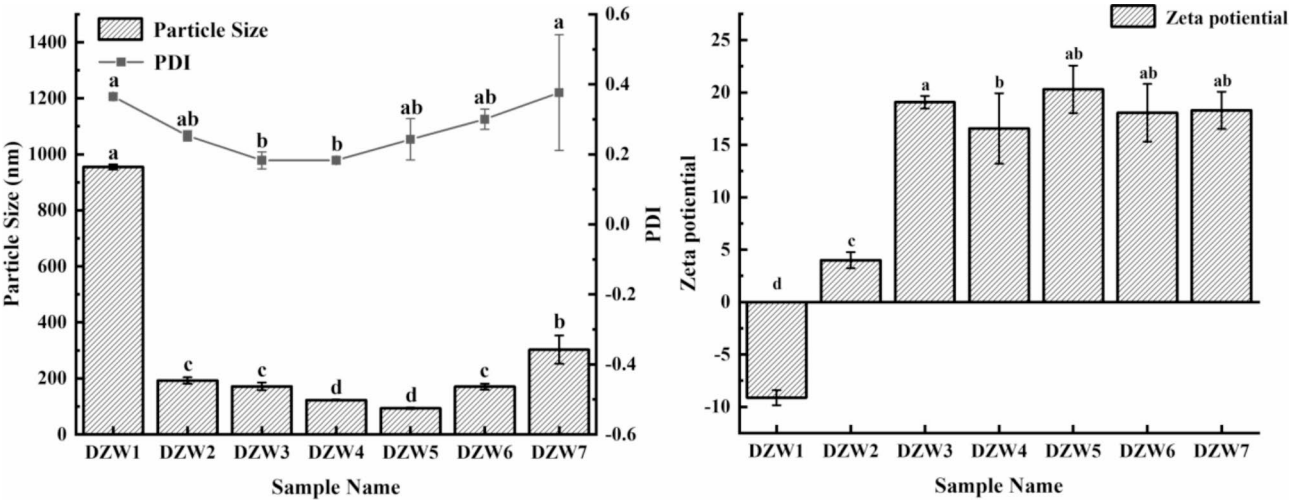

Fig. 4. The particle size, PDI and zeta potential of the DTN-loaded nanoemulsions with BgWG3 addition.

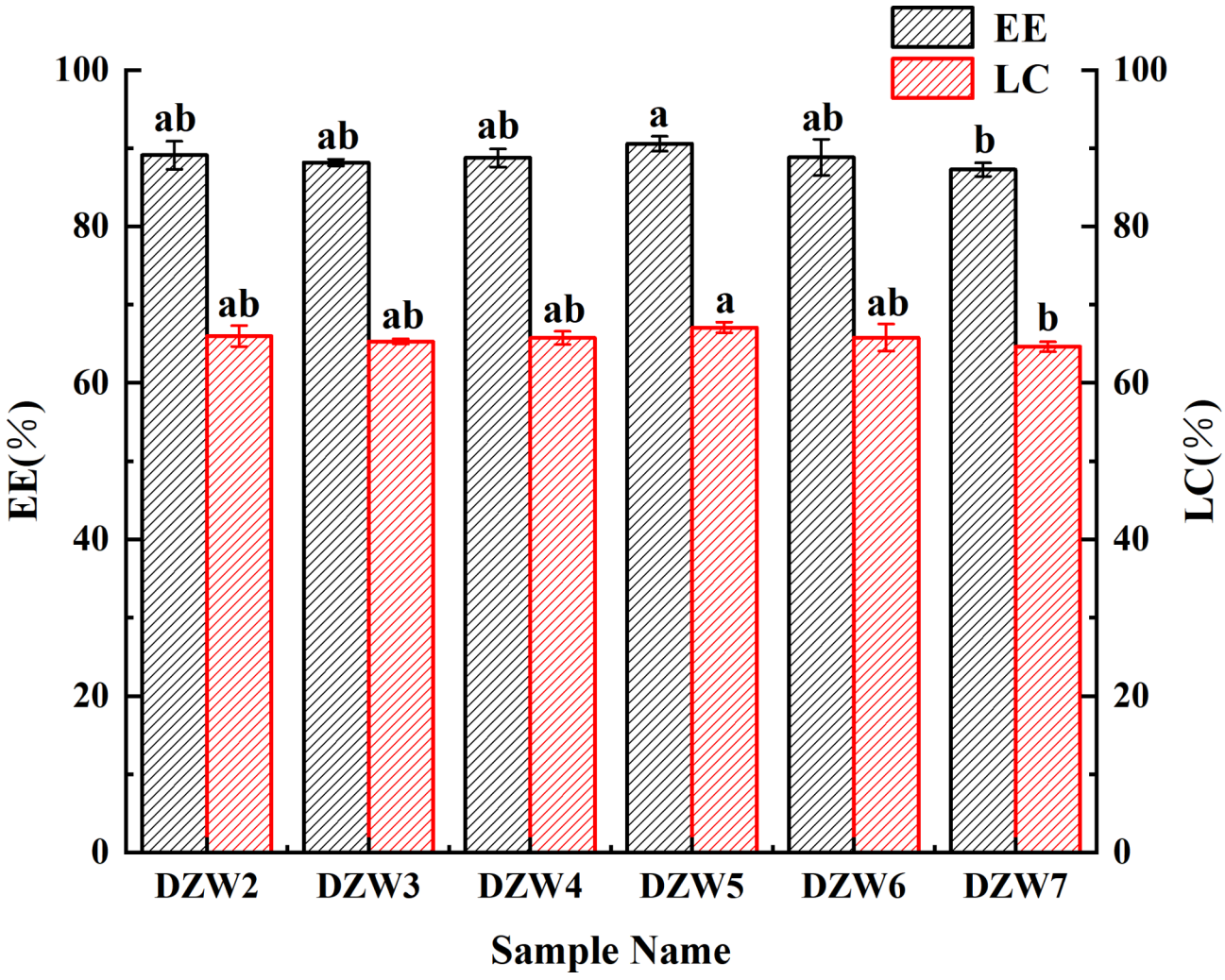

Fig. 5. Effect of modified wheat gluten addition on the EE and LC of nanoemulsions.

excessive BgWG3 disrupting emulsion interactions, a trend that aligns with the observed particle size and PDI variations.

Crystalline structure, interaction and thermal stability analysis of DTN nanoparticles

In the X-ray diffraction (XRD) patterns of the samples (Fig. 6), the Zein particles exhibit two broad diffraction peaks at 2θ = 9.31° and 19.93°, indicating an amorphous structure. DTN displays sharp single peaks at 2θ = 7.62°, 15.31°, 21.81°, and 35.12°, distinct double peaks at 19.37°/20.11°, and smaller double peaks at 23.34°/24.14°, and at 26.23°/27.12°, indicating a crystalline state[30]. After the emulsification of DZW2 and DZW4 with Zein, the single peaks at 2θ = 15.31° and 35.12° slightly decreased, and the smaller double peaks at 23.34°/24.14°, 26.23°/27.12° were notably blunted. This indicated that the DTN was encapsulated by Zein, maintaining some of the structural features of the DTN crystals.

Fluorescence spectroscopy is constantly utilized to analyze potential interaction behaviors within nanoconjugates, as intermolecular or intramolecular interactions can alter protein fluorescence properties[31]. Zein, which contains tryptophan and tyrosine residues, exhibits an emission peak at 309 nm[32]. Wheat gluten, which is more hydrophobic with a higher tryptophan to tyrosine ratio, shows an emission peak at 350 nm under 280 nm excitation[33], as depicted in Fig. 7a. Compared with that of DZW3, the fluorescence emission peak intensity of DZW5 was lower, and the maximum emission wavelength of DZW5 was redshifted relative to that of Zein, possibly because BgWG caused fluorescence quenching and irreversible structural changes in Zein[34]. Additionally, DZW5 demonstrated excellent thermal stability, with no weight loss until 170 °C, as illustrated in Fig. 7b.

Morphologies of DZW nanocapsules under TEM and SEM

The DZW2 nanoparticles, observed via TEM, are approximately 150 nm in size (Fig. 8). The addition of n-butanol to DZW2 further decreases this size to approximately 110 nm (DZW3), resulting in more uniform and dispersed particles. The size of the DZW3-DZW5 nanoparticles generally ranges from 90 to 150 nm in size, with a uniform

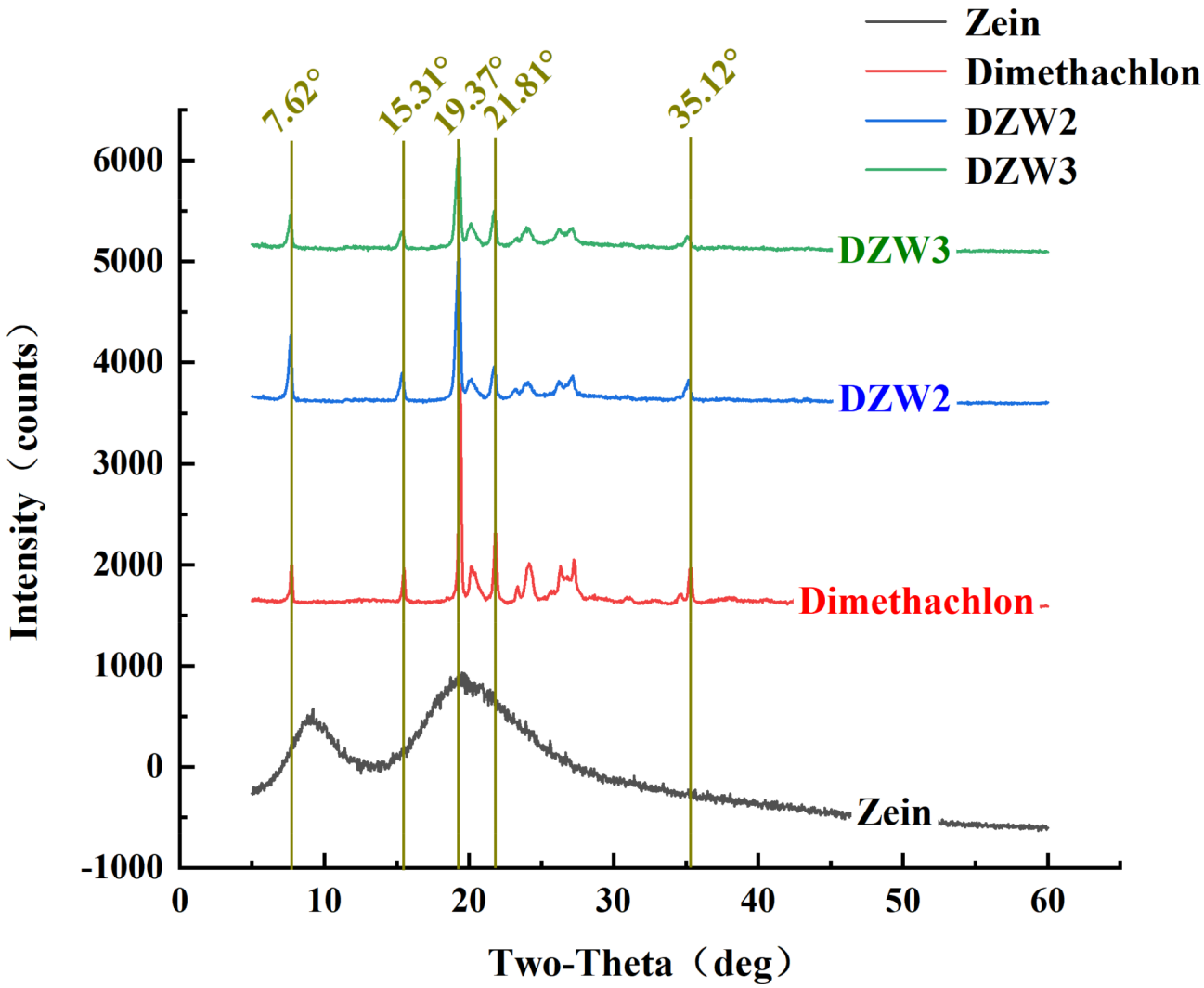

Fig. 6. XRD patterns of sample particles of nanomicroencapsulated particles.

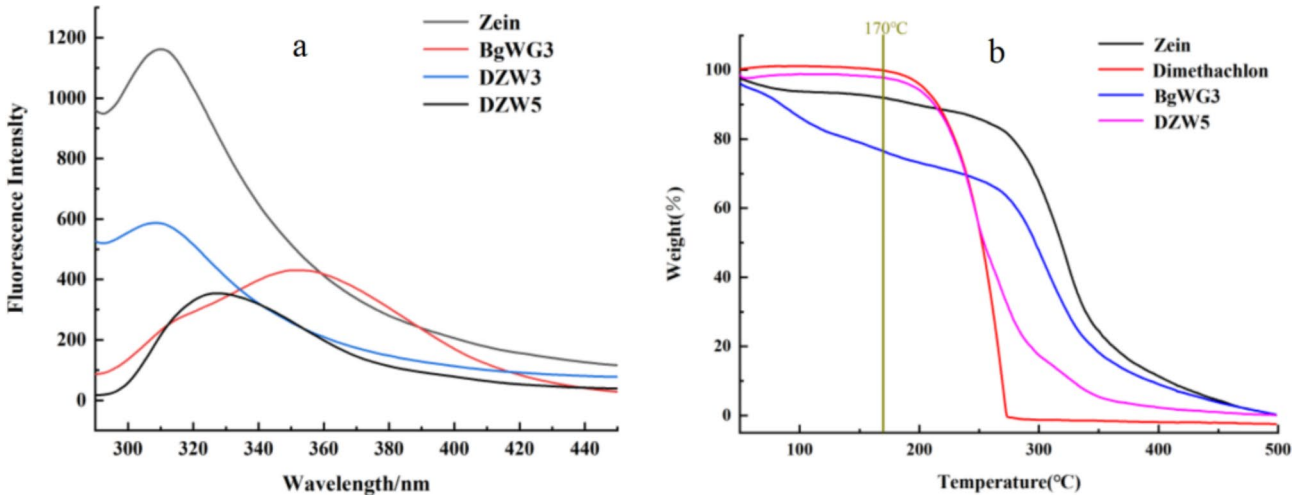

Fig. 7. the fluorescence properties and TGA analysis of Zein, DTN, BgWG3, and DTN-loaded nanoparticles.

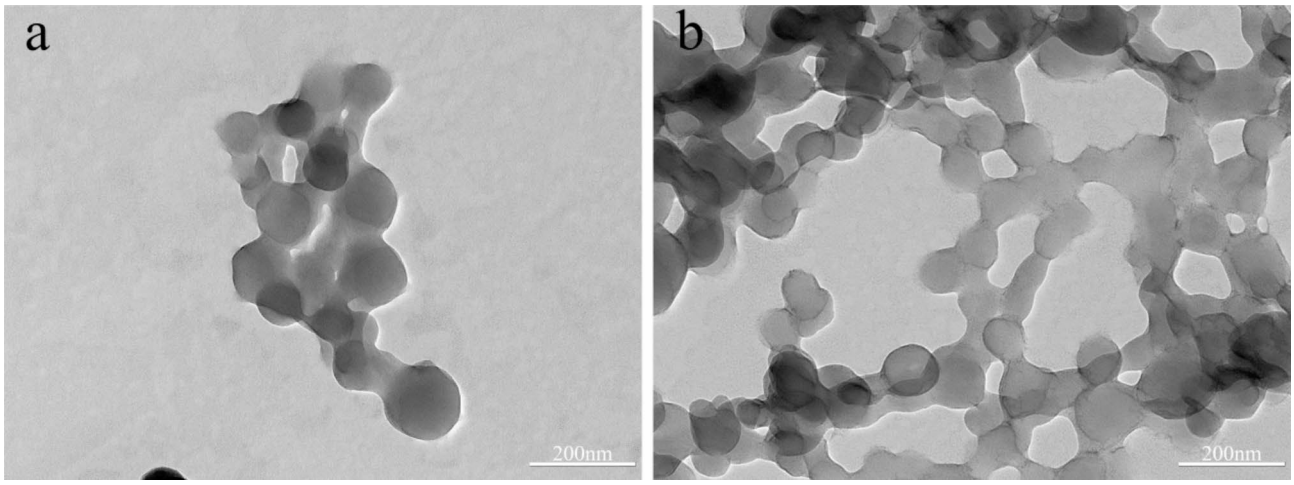

Fig. 8. TEM analysis of DTN-Zein nanoparticle samples (**a**: DZW2; **b**: DZW3).

distribution, rounded shape, and smooth surfaces, indicating effective encapsulation (Fig. 9a, b, and c). However, excessive BgWG3 increases the particle size variability, as shown in Fig. 9d. At a Zein to BgWG3 mass ratio of 3:7, the particle sizes exceeded 200 nm, with noticeable aggregation and poor dispersion. These observations align with the particle size and PDI measurements.

Characterization of DTN release properties from DZW nanoemulsions

The release profiles of the DZW nanoemulsions were assessed via dynamic dialysis. DZW1 demonstrated a significantly higher release rate than DZW2, DZW3, and DZW5 did, reaching 99.96% by 12 h (Fig. 10). The others exhibited an initial "immediate release". This early phenomenon may be attributed to phage adsorption into the nanoemulsion or DTN adsorbed on or embedded in the surface layer of the nanoparticles, leading to rapid release under concentration gradient pressure[35]. After 6 h, the release rates plateaued, with DZW2 showing the quickest release at 99.47% after 96 h. DZW3 and DZW5 had similar release rates of 94.76% and 95.67%, respectively, at 96 h. The results indicate that the addition of an appropriate amount of n-butanol improves emulsification and pesticide encapsulation, which does not impede emulsion formation, and that the pesticide release rate remains consistent.

The first-order kinetic equation $(\mathrm{Nt} = \mathrm{No}\,(1 - e^{-\mathrm{kt}}))$ was selected to model the release rate over time in the slow-release system. The release mechanism parameters—the maximum release rate (No), kinetic rate (k), correlation coefficient (R^2), and standard deviation (Se)—are listed in Table S4. The high R^2 values above 0.96 and low Se values below 0.11 for each group indicate a good fit. With respect to No. and k, DZW1 had the fastest release, followed by DZW2. DZW3 and DZW5 had significantly lower maximum release rates and slower release kinetics, suggesting a better retardation effect, which is consistent with the release curve observations described earlier.

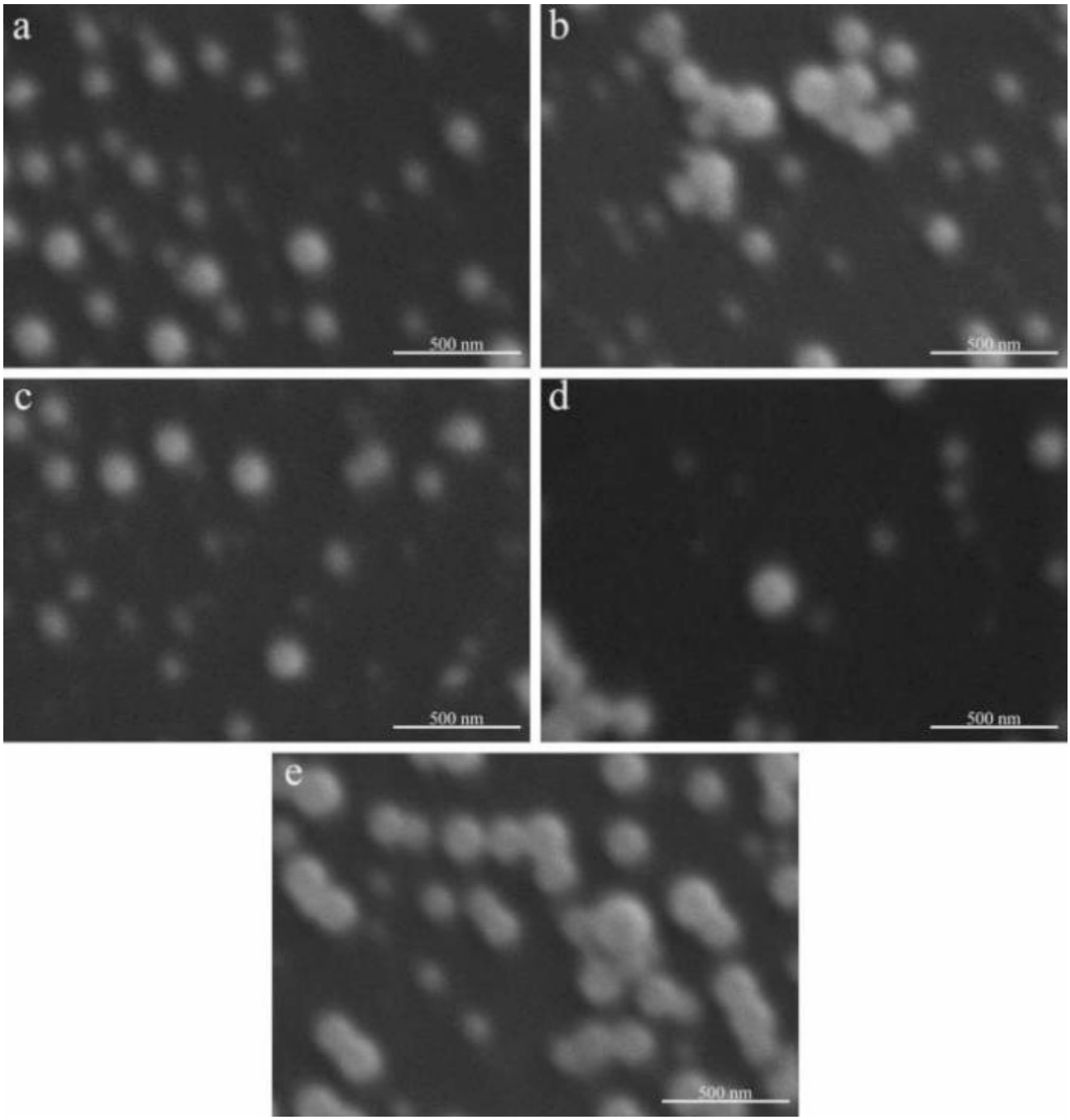

Fig. 9. SEM analysis of the DTN-Zein-modified wheat gluten nanoemulsion. (**a**: DZW3, **b**: DZW4, **c**: DZW5, **d**: DZW6, **e**: DZW7).

Combining all the above characterizations of nanoparticles such as particle size, PDI, EE, and LC, DZW5 best meets the required conditions for this study. Therefore, the DZW5 formulation was selected as the final formulation of the nanoemulsion fungicide.

Screening of biocontrol strains and susceptibility testing to DTN

F. oxysporum MLY127 hyphae are characterized by their white, fluffy appearance with a dry and dense texture, as depicted in Figure S7a, featuring curled edges and aerial hyphae. As the colonies expand, red pigmentation emerges on the periphery reverse side. The spores are ovoid or ellipsoid in the small, unicellular variety, whereas the large spores are sickle-shaped with pointed ends, as illustrated in Figure S7b and c, which aligns with the typical morphology of *F. oxysporum*[13]. The MLY127 ITS assay, sequence results, and phylogenetic tree are presented in Figure S8 of the Supplementary Material. In an antagonistic assay against *F. oxysporum* MLY127, *B. velezensis* MLY71 demonstrated a modest antagonistic effect, forming an inhibition zone approximately 0.2 cm

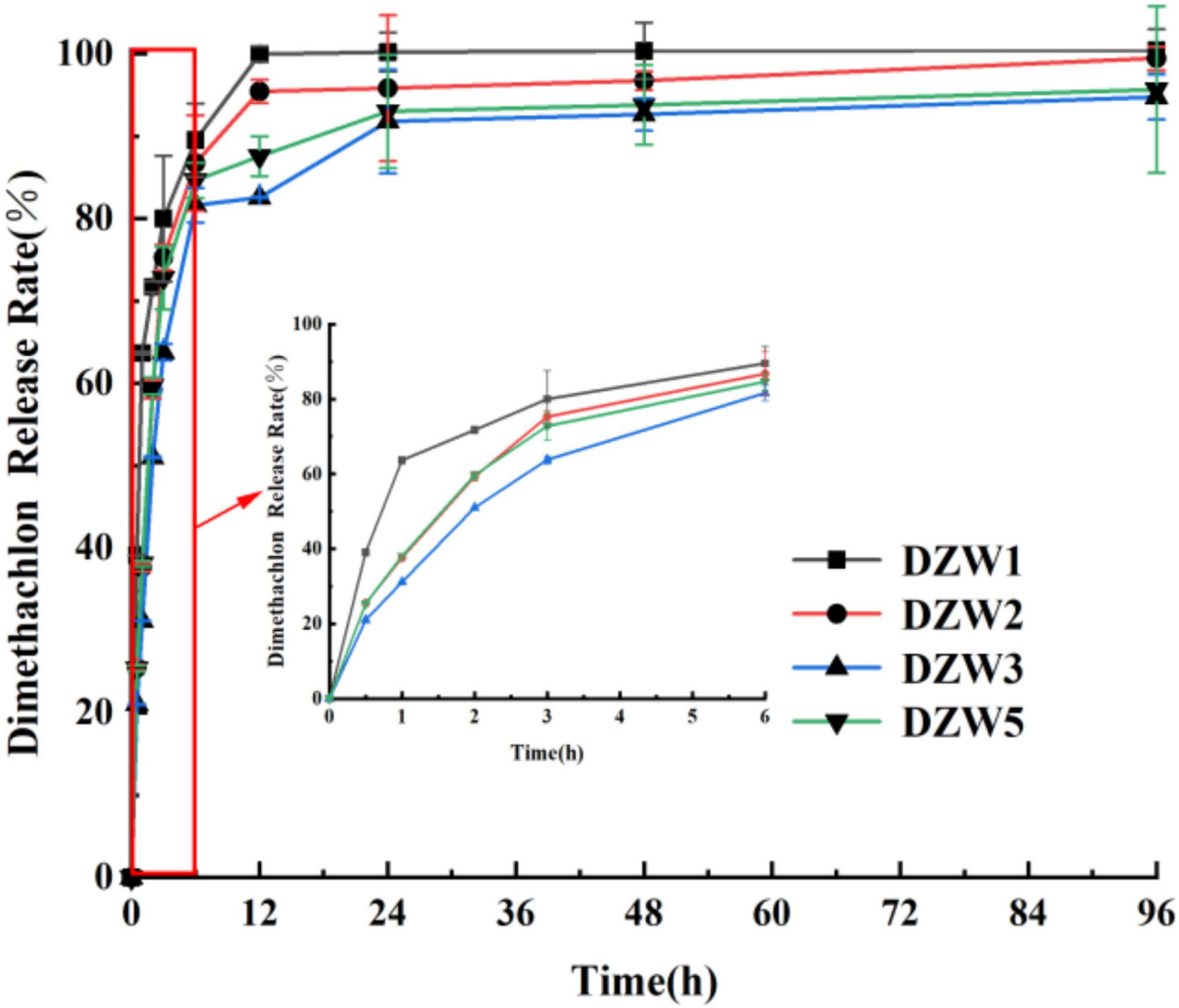

Fig. 10. DTN release profiles of different DZW nanoemulsions.

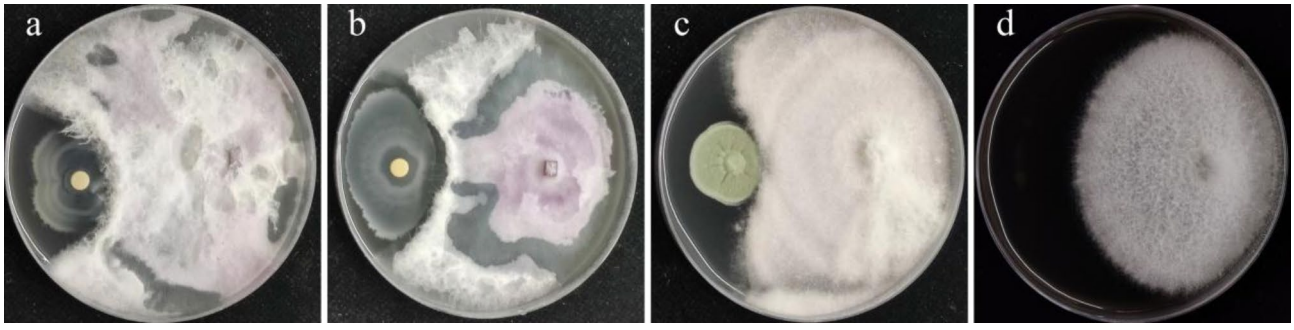

Fig. 11. Experimental plot of *F. oxysporum* MLY127 against *Bacillus amyloliquefaciens* MLY64 (**a**), *Bacillus velezensis* MLY71 (**b**) and *Penicillium citrinum* MLY85 (**c**); (**d**) is a negative control.

wide (Fig. 11), whereas MLY64 and MLY85 had negligible effects. Consequently, *B. velezensis* MLY71 was tested for sensitivity to DTN at concentrations of 0.40 mg·mL^{-1}, 0.20 mg·mL^{-1}, and 0.04 mg·mL^{-1}. No significant inhibition zones were observed (Figure S9), although 0.40 mg·mL^{-1} DTN might have slightly inhibited *Bacillus velezensis* MLY71, causing reduced bacterial growth in that region.

DZW5 nanoemulsion and *B. velezensis* MLY71 showed synergistic effects against *F. oxysporum* MLY127 both on PDYH medium and soil

The effects of the biocontrol strain-agricultural fungicide cocontrol system were assessed via the mycelial growth method (Fig. 12). The inhibitory effects of different concentrations of DTN (in DZW nanoemulsion form) and the *B. velezensis* MLY71 suspension were significantly different ($p < 0.05$) (Table S5). The combined effect of DTN and *B. velezensis* was significantly greater than their individual effects, indicating a synergistic interaction. Figure 12 shows that at lower concentrations (DTN ≤ 0.20 mg·mL^{-1}, *B. velezensis* $\leq 1 \times 10^6$ CFU·mL^{-1}), an obvious inhibition zone was observed around *F. oxysporum* MLY127. Despite the synergistic defense controlling *F. oxysporum* growth, *F. oxysporum* also inhibited the *B. velezensis* MLY71, preventing further expansion of the inhibitory effect. As the concentration increased, *B. velezensis* MLY71, aided by DTN, gained a nutritional advantage, leading to a reduction in the inhibition zone. The bacterium might produce lipopeptides, antibiotics, and other antimicrobial substances, causing *F. oxysporum* hyphae to distort and cease growth[36]. The indoor efficacy test on soil (Figure S10) confirmed that the combination of DZW5 nanoemulsion and *B. velezensis* MLY71 significantly inhibited the growth of *F. oxysporum* mycelium. The mycelium on the fungus block grew sparsely, making it difficult to effectively colonize the soil. After 14 days of cultivation, the abundance of *B. velezensis* MLY71 in the soil increased by several tens to several thousand times (Table S6). The combined application of DZW5 and *B. velezensis* MLY71 also demonstrated excellent synergistic antibacterial activity against *F. oxysporum* MLY127 in the soil. This finding suggests that the combined use of DZW5 and *B. velezensis* MLY71 should also be effective under field soil conditions. In the future, we will further conduct studies on the evaluation of disease control efficacy and the impact on soil microecology under potted and field crop conditions.

The plate antagonistic assay results, depicted in Fig. 13, revealed that the combined control of biocontrol strain-agricultural fungicides (*B. velezensis* MLY71-DZW5 nanoemulsion) over 7 days was more effective than the fungicide alone. The control effect improved with increasing concentrations of DTN. These results demonstrated that agricultural fungicides assisted biocontrol strains in gaining a colonization advantage early on, thereby increasing their survival rate. Colony growth assessments revealed an antagonistic effect at low concentrations. At a DTN concentration of 0.20 mg·mL^{-1} and a *B. velezensis* MLY71 concentration of 1×10^8 CFU·mL^{-1}, the synergistic coefficient was 1.33 (Table S7), indicating an additive effect. At greater DTN concentrations, a higher synergistic coefficient (1.77) was observed.

Discussion

Agricultural fungicides play an essential role in fungal disease control in agriculture because of their effectiveness and rapid action. However, a shift toward developing safer and more efficient formulations, such as water-based, nanosized, ultralow-volume, and slow-release types, to decrease chemical usage and foster greener control methods[9,37–39] has been promoted because of the implementation of pesticide reduction policies. Owing to their small size, high biocompatibility, and large surface area, nanomaterials offer advantages in creating nanoparticle-based plant protection agents. These agents can improve the environmental stability and efficacy of plant protection factors against pests and diseases[39,40]. The test results indicate that DTN in the DZW nanocarrier has a slow-release profile, maintaining effective release for up eight times longer than its aqueous counterpart. This extended release significantly enhances the field stability of DTN, mitigating dilution by rainfall and increasing pesticide utilization efficiency.

Bacillus spp. possess a range of biocontrol capabilities and are promising for bioprevention applications because of their safety, eco-friendliness, broad antimicrobial action, and ability to promote plant growth[36]. Currently, they are being studied for their ability to control rice blast caused by *Magnaporthe oryzae*, tomato late blight caused by *Phytophthora infestans*, tomato wilt disease caused by *F. oxysporum* f. sp. *lycopersici*, and verticillium wilt of cotton caused by *F. oxysporum* f. sp. *vasinfectum*[41–43]. Several studies have reported that *Bacillus* spp. and synthetic fungicides have enhanced antimicrobial effects against fungi when used together. For example, Abo-Elyousr et al. reported that a combination of *B. subtilis* and benzothiadiazole significantly increased resistance to *F. oxysporum* by reducing disease severity[44]. Similarly, Chen et al. demonstrated a good synergistic effect of *B. velezensis* SDTB038 and phenamacril against *F. oxysporum* f. sp. in tomato root rot control[45]. This study also revealed that the synergistic effect of *B. velezensis* MLY71 with DTN on *F. oxysporum* MLY127 was notably greater than that of single treatments. At a bacterial concentration of 1×10^4 CFU·mL^{-1} and a DTN concentration of 0.04 mg·mL^{-1}, the combined inhibition rate reached 76.66%. This could reduce the application concentration and amount of DTN in agriculture, thereby decreasing its residue and toxicity to the soil. Additionally, chemical fungicides can assist biocontrol strains in overcoming the soil ecological environment, aiding in colonization and establishing population advantages, which improves the survival of biocontrol strains and the stability of biological control[10].

Zein as a raw material is a common plant protein known for its nontoxicity, renewability, and biodegradability, and it offers excellent biocompatibility and unique hydrophobic properties as a carrier. Its structure, which is composed of approximately 75% hydrophobic and 25% hydrophilic amino acids, confers amphiphilicity, allowing it to dissolve in ethanol concentrations of 60–90% and self-assemble into nanoparticles. These nanoparticles are superior carriers for hydrophobic pesticides[46–49]. Zein nanoparticles increase pesticide stability, utilization, and control release, making them ideal for fungicide encapsulation to achieve controlled release and enhanced therapeutic efficacy in research applications. However, high-purity Zein is expensive, often making it unaffordable for farmers because of high production costs. In contrast, wheat gluten, a low-cost byproduct of wheat processing, contains approximately 80% protein, along with small amounts of lipids, carbohydrates, and minerals[50,51]. It also exhibits surface-active properties such as emulsification, foaming, and surface tension, similar to Zein[52]. However, the solubility of wheat gluten is limited by its high content of hydrophobic amino acids, as well as both negatively charged amino acids (glutamic acid) and positively charged amino acids (glutamine, arginine and lysine), which form crosslinks and large hydrophobic regions, affecting its surface properties and making

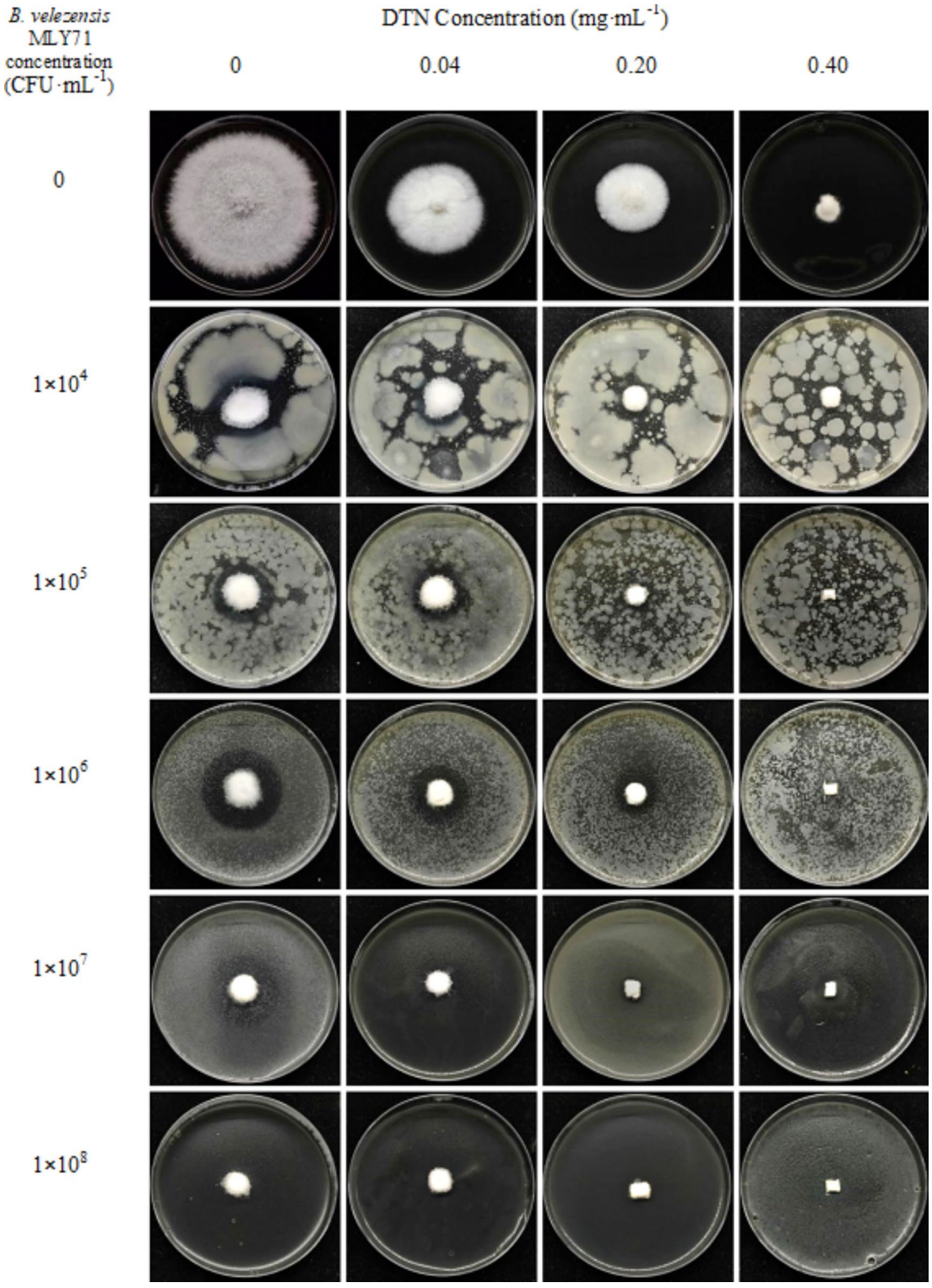

Fig. 12. Efficacy of the combination of DZW5 nanoemulsion and *B. velezensis* MLY71 strain against *F. oxysporum* MLY127.

it unsuitable for some production needs[53,54]. To address this, we grafted modified wheat gluten with BZH to consume positively charged amidogen groups to reduce internal and internal electrostatic cross-linking and enhance its functional properties and amphiphilicity, meeting the application requirements[55]. The modification significantly improved the solubility and demonstrated satisfactory emulsification and stability for the test. The appropriate amount of additive can further reduce the nanoparticle size and increase the nanoemulsion stability. Additionally, it improved the EE and LC, leading to better DTN encapsulation for DZW. This mode of simple

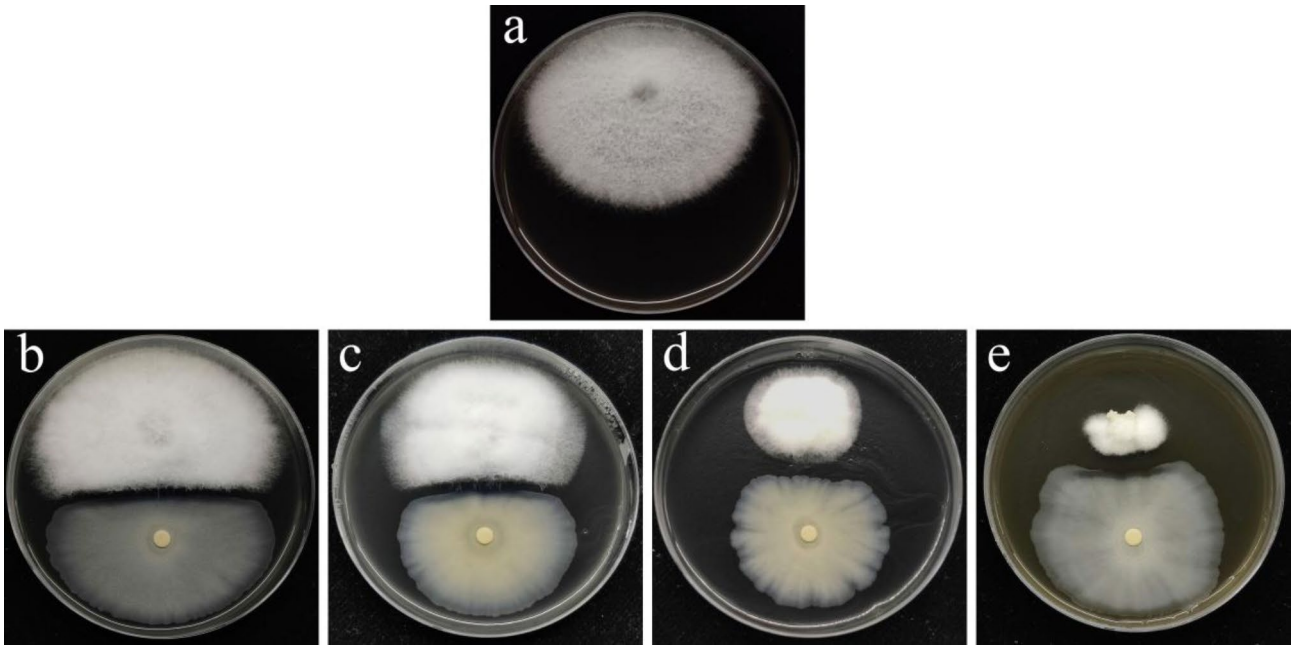

Fig. 13. Determination of the synergistic effects of DTN and *B. velezensis* MLY71 against *F. oxysporum* MLY127 via a plate antagnostic assay. (**a**: control; **b**: Dimethachlon concentration of 0 mg·mL^{-1}; **c**: Dimethachlon concentration of 0.04 mg·mL^{-1}; **c**: Dimethachlon concentration of 0.20 mg·mL^{-1}; **d**: Dimethachlon concentration of 0.40 mg·mL^{-1}).

production and lower production cost is more suitable for application promotion in agricultural production, and at the same time, it can provide a more practical reference for the field of agricultural control.

Moreover, the protein-based nanocarriers used can serve as a nitrogen source for crops and benefit soil microorganisms. Although this study did not involve field application or soil microbial analysis, the literature suggests that proteins can enrich the soil microbial environment around crops[56] and that organic nitrogen can be directly absorbed by crop roots[57], aiding in chlorophyll synthesis, improving plant health, and promoting growth.

Conclusion

In this study, wheat gluten was grafted with BZH to improve its solubility in water and alcohol through the addition of alcohol-soluble benzyl groups, increasing its emulsification capacity. The optimal formulation for the DZW nanoemulsion was selected through component ratio screening. *F. oxysporum* MLY127 was isolated from diseased tobacco stems, and *B. velezensis* MLY71, which is antagonistic to this strain, was obtained through screening. The study achieved synergistic enhancement of *F. oxysporum* MLY127 growth inhibition via combination of *B. velezensis* MLY71 and the DZW nanoemulsion. Notably, the DZW nanopreparation demonstrated sustained release for 96 h, extending the application time eightfold compared with that of the aqueous agent. The DZW nanopreparation, in combination with *B. velezensis* MLY71, formed a synergistic control system, reaching over 75% inhibition rate at bacterial concentrations of 1×10^4 CFU/mL and DTN concentrations of 0.04 mg·mL^{-1}. At a DTN concentration of 0.20 mg·mL^{-1}, the DZW nanopreparation showed synergistic inhibition against *F. oxysporum* MLY127. This synergistic effect of fungicide-biocontrol microbe combinations offers essential technical support for increased field efficacy in subsequent applications and provides valuable references for the development of more fungicide-biocontrol strain combinations.

Data availability

Data is provided within the manuscript or supplementary information files.

Received: 4 July 2024; Accepted: 26 November 2024
Published online: 02 December 2024

References

1. Alexander, K., Anastasia, S., Tatyana, R., Michael, B., Anton, L. The Genome Sequence of Five Highly Pathogenic Isolates of *Fusarium oxysporum* f. sp. lini. *Molecular plant-microbe interactions : MPMI* **33**, MPMI05200130SC. https://doi.org/10.1094/MPMI-05-20-0130-SC (2020).
2. Di, P. A., P, M. M., Zaira, C., Jesús, D.-J., G, R. M. I. *Fusarium oxysporum*: exploring the molecular arsenal of a vascular wilt fungus. *Molecular plant pathology* **4**, 315–325. https://doi.org/10.1046/j.1364-3703.2003.00180.x (2003).
3. B, M. C., Martijn, R. Pathogen profile update: *Fusarium oxysporum*. *Molecular plant pathology* **10**, 311–324. https://doi.org/10.1111/j.1364-3703.2009.00538.x (2009).

4. Kumar, S. *et al.* Nanobased smart pesticide formulations: Emerging opportunities for agriculture. *Journal of Controlled Release* **294**, 131–153. https://doi.org/10.1016/j.jconrel.2018.12.012 (2019).
5. Maira, L., Eleftheria, B., Filitsa, K., A., A. K. Do pesticides promote or hinder sustainability in agriculture? The challenge of sustainable use of pesticides in modern agriculture. *Science of the Total Environment* **795**, 148625–148625. https://doi.org/10.1016/j.scitotenv.2021.148625 (2021).
6. Karamchandani, B. M., Dalvi, S. G., Bagayatkar, M., Banat, I. M., Satpute, S. K. Prospective applications of chitosan and chitosan-based nanoparticles formulations in sustainable agricultural practices. *Biocatalysis and Agricultural Biotechnology* **58**, 103210-. https://doi.org/10.1016/j.bcab.2024.103210 (2024).
7. Jiaming, Y., Xiaofeng, S., Shuo, Y., Jie, S. Multifunctional Nanoparticles and Nanopesticides in Agricultural Application. *Nanomaterials (Basel, Switzerland)* **13**. https://doi.org/10.3390/NANO13071255 (2023).
8. Wahab, A. *et al.* Agriculture and environmental management through nanotechnology: Eco-friendly nanomaterial synthesis for soil–plant systems, food safety, and sustainability. *The Science of the total environment* **926**, 171862–171862. https://doi.org/10.1016/J.SCITOTENV.2024.171862 (2024).
9. Mali, S. C., Raj, S., Trivedi, R. Nanotechnology a novel approach to enhance crop productivity. *Biochemistry and Biophysics Reports* **24**, 100821–100821. https://doi.org/10.1016/j.bbrep.2020.100821 (2020).
10. Katan, J., Ginzburg, C., Freeman, S. The weakening effect as a trigger for biological control and criteria for its evaluation. *Biological Control of Plant Diseases* pp 55–61. https://doi.org/10.1007/978-1-4757-9468-7_6 (1992).
11. Khan, M., Salman, M., Jan, S. A., Shinwari, Z. K. Biological Control of Fungal Phytopathogens: A Comprehensive Review Based on Bacillus Species. *Biology and Medicine* **6**, 90–92. https://doi.org/10.15406/mojbm.2021.06.00137 (2021).
12. Pinckney, A. The biuret test as applied to the estimation of wheat protein. *Cereal Chemistry* **38**, 501–506. https://doi.org/10.1007/978-3-031-50643-7_18 (1961).
13. Garrido, P. C. *et al.* Using Redox Proteomics to Gain New Insights into Neurodegenerative Disease and Protein Modification. *Antioxidants* **13**, 127-. https://doi.org/10.3390/antiox13010127 (2024).
14. Schacterle, G. R., Pollack, R. L. A simplified method for the quantitative assay of small amounts of protein in biologic material. *Analytical Biochemistry* **51**, 654–655. https://doi.org/10.1016/0003-2697(73)90523-x (1973).
15. Pei-Jia Lu *et al.* Methodology for sample preparation and size measurement of commercial ZnO nanoparticles. *Journal of Food and Drug Analysis* **26**, 628–636. https://doi.org/10.1016/j.jfda.2017.07.004 (2018).
16. Julio M. Frasca, Parks, V. R. A routine technique for double-staining ultrathin sections using uranyl and lead salts. *Journal of Cell Biology* **25**, 157–161. https://doi.org/10.1083/jcb.25.1.157 (1965).
17. Zhou, G. *et al.* A new drug-loading technique with high efficaciency and sustained-releasing ability via the Pickering emulsion interfacial assembly of temperature/pH-sensitive nanogels. *Reactive and Functional Polymers* **73**, 1537–1543. https://doi.org/10.1016/j.reactfunctpolym.2013.08.004 (2013).
18. Lin, Y. *et al.* Development of 1,3,4-Oxadiazole Derived Antifungal Agents and Their Application in Maize Diseases Control&#13. *Frontiers in Plant Science* **13**, 912091–912091. https://doi.org/10.3389/fpls.2022.912091 (2022).
19. Ma, Z., Niu, F., Bi, Q. A method for evaluating the combined synergistic effect of Mycosphaerella Hartz and chemical pesticides. *Agrochemical* **52**, 921–923. https://doi.org/10.16820/j.cnki.1006-0413.2013.12.022 (2013).
20. Fevzioglu, M., Ozturk, O. K., Hamaker, B. R., Campanella, O. H. Quantitative approach to study secondary structure of proteins by FT-IR spectroscopy, using a model wheat gluten system. *International Journal of Biological Macromolecules* **164**, 2753–2760. https://doi.org/10.1016/j.ijbiomac.2020.07.299 (2020).
21. Molina, E., Papadopoulou, A., Ledward, D. A. Emulsifying properties of high pressure treated soy protein isolate and 7S and 11S globulins. *Food Hydrocolloids* **15**, 263–269. https://doi.org/10.1016/S0268-005X(01)00023 – 6 (2001).
22. Xie, M., Liu, Y. Infrared spectroscopy of amide III bands for protein secondary structure determination studies. *Journal of Higher Education Chemistry.* **2**, 226–231. (2003).
23. Pham, P., Oliver, S., Wong, E. H. H., Boyer, C. Effect of hydrophilic groups on the bioactivity of antimicrobial polymers. *Polymer Chemistry* **12**, 5689–5703. https://doi.org/10.1039/D1PY01075A (2021).
24. Sameer, K., Reda, R., Khalid, K., Gwo-Yu, C., Halima, B. DeepSol: a deep learning framework for sequence-based protein solubility prediction. *Bioinformatics (Oxford, England)* **34**, 2605–2613. https://doi.org/10.1093/bioinformatics/bty166 (2018).
25. Koop, J., Merz, J., Pietzsch, C., Schembecker, G. Contribution of Secondary Structure Changes to the Surface Activity of Proteins. *Journal of Biotechnology* **323**, 208–220. 10.1016/j.jbiotec.2020.07.015 (2020).
26. Lu, C. *et al.* Behavior of the 2,4-distyryl saturated cardanol PPO-PEO-SO3 – surfactant at the oil/water interface through molecular dynamics simulations. *Journal of Molecular Liquids* **397**, 124156-. https://doi.org/10.1016/j.molliq.2024.124156 (2024).
27. Meng, R., Wu, Z., Xie, Q.-T., Cheng, J.-S., Zhang, B. Preparation and characterization of zein/carboxymethyl dextrin nanoparticles to encapsulate curcumin: Physicochemical stability, antioxidant activity and controlled release properties. *Food Chemistry* **340**, 127893–127893. (2021).
28. K, R. M., N, P. J., Rodolphe, M. Size and surface charge characterization of nanoparticles with a salt gradient. *Nature communications* **11**, 2337. 10.1038/s41467-020-15889-3 (2020).
29. A., S.-L. *et al.* Zeta potential as a tool for functional materials development. *Catalysis Today*, **423**. https://doi.org/10.1016/j.cattod.2022.08.004 (2023).
30. Schmid, A., Tonnar, J., Armes, S. P. A New Highly Efficient Route to Polymer-Silica Colloidal Nanocomposite Particles. *Advanced Materials* **20**, 3331–3336. https://doi.org/10.1002/adma.200800506 (2008).
31. S, S. H. K., Pilar, G. M. d., Javier, G. Effect of chitosan degradation on its interaction with β-lactoglobulin. *Biomacromolecules* **12**, 1015–1023. https://doi.org/10.1021/bm101356g (2011).
32. Albani, J. R. Structure and dynamics of macromlecules: a bsorption and fluorescence studies: absorption and fluorescence studies. *Elsevier Science* **4**, 387–407. https://doi.org/10.1016/b978-0-444-51449-3.x5000-x (2005).
33. Wang, Y., Gan, J., Zhou, Y., Cheng, Y., Nirasawa, S. Improving solubility and emulsifying property of wheat gluten by deamidation with four different acids: Effect of replacement of folded conformation by extended structure. *Food Hydrocolloids* **72**, 105–114. https://doi.org/10.1016/j.foodhyd.2017.04.013 (2017).
34. Datta, D., Swamy, M. J. Fluorescence and circular dichroism studies on the accessibility of tryptophan residues and unfolding of a jacalin-related α- d -galactose-specific lectin from mulberry (Morus indica). *Journal of Photochemistry & Photobiology, B: Biology* **170**, 108–117. https://doi.org/10.1016/j.jphotobiol.2017.03.026 (2017).
35. Wei, Z., Yang, W., Fan, R., Yuan, F., Gao, Y. Evaluation of structural and functional properties of proteinâ EGCG complexes and their ability of stabilizing a model Î²-carotene emulsion. *Food Hydrocolloids* **45**, 337–350. 10.1016/j.foodhyd.2014.12.008 (2015).
36. Bhairav, P., Deepak, S., Pankaj, K., Ramesh, C. D. Biocontrol potential of Bacillus spp. for resilient and sustainable agricultural systems. *Physiological and Molecular Plant Pathology* **128**. https://doi.org/10.1016/j.pmpp.2023.102173 (2023).
37. Dasgupta, N. *et al.* Nanotechnology in agro-food: From field to plate. *Food Research International* **69**, 381–400. https://doi.org/10.1016/j.foodres.2015.01.005 (2015).
38. Haris, M. *et al.* Nanotechnology - A new frontier of nanofarming in agricultural and food production and its development. *Science of The Total Environment* **857**, 159639. https://doi.org/10.1016/j.scitotenv.2022.159639. (2023).
39. Tomar, P. *et al.* Bacterial biopesticides: Biodiversity, role in pest management and beneficial impact on agricultural and environmental sustainability. *Heliyon* **10**, e31550-. https://doi.org/10.1016/j.heliyon.2024.e31550 (2024).
40. Branislav, R.-N., Olga, K., Lukas, N., Vojtech, A. Nanoparticles based on essential metals and their phytotoxicity. *Journal of nanobiotechnology* **15**, 33. https://doi.org/10.1186/s12951-017-0268-3 (2017).

41. Abdallah, R. A. B. *et al.* Involvement of lipopeptide antibiotics and chitinase genes and induction of host defense in suppression of Fusarium wilt by endophytic Bacillus spp. in tomato. *Crop Protection* **99**, 45–58. https://doi.org/10.1016/j.cropro.2017.05.008 (2017).
42. Dhouib, H. *et al.* Potential of a novel endophytic Bacillus velezensis in tomato growth promotion and protection against Verticillium wilt disease. *Biological Control* **139**, 104092–104092. https://doi.org/10.1016/j.biocontrol.2019.104092 (2019).
43. Nihorimbere, G. *et al.* Bacillus-based biocontrol beyond chemical control in central Africa: the challenge of turning myth into reality. *Frontiers in Plant Science* **15**, 1349357–1349357. https://doi.org/10.3389/fpls.2024.1349357 (2024).
44. M., A. E. K. A., M.A, S. N., A, M. M. A., Muhammad, I., R., A. R. I. Synergistic effect of *Bacillus subtilis* and benzothiadiazole (Bion®) on the suppression of *Fusarium oxysporum* and the enhancement of disease resistance in Capsicum annuum. *Journal of Plant Pathology***106**, 127–138. https://doi.org/10.1007/s42161-023-01527-6 (2023).
45. Chen, Q. *et al.* Synergistic effects of Bacillus velezensis SDTB038 and phenamacril on Fusarium crown and root rot of tomato. *Plant Pathology* **72**, 1453–1462. 10.1111/ppa.13769 (2023).
46. Elzoghby, A. O., Samy, W. M., Elgindy, N. A. Protein-based nanocarriers as promising drug and gene delivery systems. *Journal of Controlled Release* **161**, 38–49. https://doi.org/10.1016/j.jconrel.2012.04.036 (2012).
47. Sanghoon, K., C., P. S. Optimal conditions for the encapsulation of menthol into zein nanoparticles. *LWT* **144**. https://doi.org/10.1016/j.lwt.2021.111213 (2021).
48. Tao, Z. *et al.* Ethanol-soluble polysaccharide from sugar beet pulp for stabilizing zein nanoparticles and improving encapsulation of curcumin. *Food Hydrocolloids* **124**. 10.1016/j.foodhyd.2021.107208 (2022).
49. YongJin, K. *et al.* Zein-Induced Polyelectrolyte Complexes for Encapsulating Triterpenoid Phytochemicals. *ACS omega* **8**, 44637–44646. https://doi.org/10.1021/acsomega.3c05157 (2023).
50. Peña, E., Bernardo, A., Soler, C., Jouve, N. Relationship between common wheat (*Triticum aestivum L.*) gluten proteins and dough rheological properties. *Euphytica* **143**, 169–177. https://doi.org/10.1007/s10681-005-3157-z (2005).
51. Aminzare, M. *et al.* Characteristics, antimicrobial capacity, and antioxidant potential of electrospun zein/polyvinyl alcohol nanofibers containing thymoquinone and electrosprayed resveratrol nanoparticles. *Food science & nutrition* **12**, 1023–1034. https://doi.org/10.1002/fsn3.3816 (2024).
52. Qiu, C., Sun, W., Zhao, Q., Cui, C., Zhao, M. Emulsifying and surface properties of citric acid deamidated wheat gliadin. *Journal of Cereal Science* **58**, 68–75. https://doi.org/10.1016/j.jcs.2013.04.002 (2013).
53. Wrigley, C., Bushuk, W., Gupta, R. Nomenclature: establishing a common gluten language. *Melbourne* **1996**, 403–407. (1996).
54. Siddiqi, R. A., Singh, T. P., Rani, M., Sogi, D. S., Bhat, M. A. Diversity in Grain, Flour, Amino Acid Composition, Protein Profiling, and Proportion of Total Flour Proteins of Different Wheat Cultivars of North India. *Frontiers in Nutrition* **7**, 141. https://doi.org/10.3389/fnut.2020.00141 (2020).
55. Zhenyuan, L. *et al.* Properties of wheat gluten based wood adhesives enhanced by transglutaminase and epichlorohydrin. *International Journal of Adhesion and Adhesives* **130**, 103607-. https://doi.org/10.1016/j.ijadhadh.2023.103607 (2024).
56. Raju, I., Pandian, K., Ramalingam, A., Ramaiyer, L. M. Soil Proteomics: Diversity and Functions. *Structure and Functions of Pedosphere*, pp: 411–427. https://doi.org/10.1007/978-981-16-8770-9_17 (2022).
57. Chanyarat, P.-L. *et al.* Plants can use protein as a nitrogen source without assistance from other organisms. *Proceedings of the National Academy of Sciences of the United States of America* **105**, 4524–4529. https://doi.org/10.1073/pnas.0712078105 (2008).

Acknowledgements

Anonymous reviewers are gratefully acknowledged for their constructive review that signifcantly improved this manuscript. The authors also would like to thank Qian Yang from the analysis and testing center of the Zhejiang University of Technology for the TEM test.

Author contributions

Conceptualization, L.Y., Y.L.; methodology, L.Y., J.G., X.D., X.H., and G.L.; formal analysis, Y.L., and G.L.; investigation, Y.L. and J.G.; resources, L.Y., X.D., and X.H.; writing—original draft preparation, Y. L., and J.G.; writing—review and editing, Y.L.; supervision, L.Y.; project administration, L.Y. and Y.L.; funding acquisition, L.Y. and Y.L. All authors have read and agreed to the published version of the manuscript.

Declarations

Competing interests

The authors declare no competing interests.

Additional information

Supplementary Information The online version contains supplementary material available at https://doi.org/10.1038/s41598-024-81356-4.

Correspondence and requests for materials should be addressed to Y.L.

Reprints and permissions information is available at www.nature.com/reprints.

Publisher's note Springer Nature remains neutral with regard to jurisdictional claims in published maps and institutional affiliations.